# Progress Report: Neural Networks for Computed Tomography Imaging Spectroscopy of the Solar Atmosphere

Roy Smart
roy.smart@montana.edu
Montana State University, Department of Physics
Bozeman, MT 59717, USA

March 6, 2018

## 1 Introduction

The goal of this investigation is to classify explosive events (EEs) in the solar transition region (TR) using snapshot imaging spectroscopy. We proposed to accomplish this goal using observations from two snapshot imaging spectrographs, the *Multi-order Solar EUV Spectrograph* (MOSES), and the *EUV Snapshot Imaging Spectrograph* (ESIS), of which MOSES has successfully flown in 2006 and 2015, and ESIS is scheduled to launch alongside MOSES in 2019.

These spectrographs are unique in that they have the capability to spectrally-resolve a few extreme ultraviolet (EUV) emission lines over a large 2D field-of-view (FOV). However, this capability depends on the development of robust inversion algorithms that can interpret the data correctly. Therfore, the integral part of our proposal was the development of a convolutional neural network (CNN)-based inversion algorithm that used the IRIS Si IV 1403 Å spectral observations as a model for the EUV emission lines observed by MOSES and ESIS.

During the course of our investigation, we found that achieving a full spectrum inversion superior to those demonstrated in the proposal would require a more sophisticated network than previously anticipated. This modification will be discussed in Section 3.2, but we were able to build a useful network using our proposed architecture, a central-tendency neural network. Instead of reconstructing the full spectrum, this network simply reconstructs the central-tendency (bulk doppler shift), which is a much easier problem to solve. Unfortunately, out central-tendency network is easily confounded by spikes in the training set, which necessitated the development of a high-performance image despking routine, discussed in Section 2.1.2.

## 2 Progress Report

While the development of inversion routines is the most discussed milestone of this investigation, assembling the MOSES and ESIS instruments for flight in 2019 is an important goal of my research group. My most significant objective in the instrument assembly is the optical alignment and focus of both ESIS and MOSES. This effort has provided much needed experience using the instruments in this study, which will allow us to be more effective in the development of our inversion routines.

Parallel to the advancement of MOSES and ESIS, I was also involved in the design phase of the FURST mission, which was just accepted in this latest LCAS proposal round. The design process of FURST gave me useful experience using optical modeling software, which will allow for the implementation of more sophisticated instrument models in our inversion routine.

## 2.1 CTIS Inversion Neural Networks

Since the ultimate goal of solar spectroscopy is the determination of plasma parameters such as bulk velocity, temperature, density, etc., we don't necessarily need to recover the spectrum from MOSES observations, just the derived physical quantities that we're interested in. Finding a few physical quantities is easier than reconstructing the entire spectrum since they contain less information, easing the ill-posedness of the inversion problem. Contrary to the plan outlined in the NESSF17 proposal, we decided to first construct a neural network that would derive the bulk velocity of TR plasma by finding the central-tendency (doppler shift) of an input spectrum from a MOSES observation.

This branch from the proposal was temporarily taken since we wanted to be sure that we could solve this simple problem before putting too much effort into a full spectrum inversion. From the development of our Doppler inversion network (DIN), we were able to see the necessity of a high-performance despiking algorithm for the input dataset. We have nearly completed a pixel-identification module of our despiking alogrithm, and are planning a simple implementation of a pixel replacement module.

### 2.1.1 Doppler Inversion Network

Our DIN is a sophisticated 21x21 kernel that is convolved with MOSES observations to yield the Doppler shift at each pixel. The convolutional kernel is learned through training on MOSES observations where the Doppler shift at each pixel is known a priori. This a priori dataset is formed by using the IRIS Si IV 1403 Å spectral line as model for the He II 304 Å line observed by MOSES. The Doppler shift is taken to be the mean along the spectral dimension of the IRIS observations in a -150 to 150 km/s window centered around the Si IV 1403 Å spectral line.

During the development of our DIN, we tested two neural networks to understand how increasing the complexity of the network affects the quality of the results. The first network was dubbed the "test" network, and contained relatively few free parameters, while the "Final" network had many more free parameters, to increase the predictive power of the network. In Table 1, we have provided both parameters and results of both networks. Here, we can see that both networks were able to achieve an RMS velocity error better than the theoretical resolution of MOSES (29 km/s).

| | Test | Final |
|---|---|---|
| Free Parameters | 1.2k | 836k |
| Training Images | 4.5k | 4.5k |
| Training time (min) | 3 | 15 |
| RMS error (km/s) | 12.7 | 10.3 |
| Pearson's $r$ | 0.500 | 0.701 |

Table 1: Description of the characteristics and results of two neural networks tested for this progress report. More comprehensive results from the "Final" network are presented in later figures.

In Figure 1 we have provided a few validation examples of our method, where we have plotted the reconstructed Doppler velocity along with the "true" velocity for comparison. We chose to show these validation examples since they demonstrated reasonably-high Doppler velocities, characteristic of some types of EEs We can see that in areas of high signal the network does reasonably well at reproducing the true Doppler shift, while in areas of low signal the Doppler shift is underestimated. We anticipate that the despiking procedure outlined in Section 2.1.2 will improve results in these low-signal areas, since spikes are more effective at changing the estimated Doppler shift in these areas.

In Figure 2b we constructed a histogram of the true velocity vs. the reconstructed velocity for every pixel in our validation dataset to demonstrate the statistical effectiveness of our method. If the DIN reconstruction were perfect, the result of this plot would be a straight line with slope unity (plotted in blue). Immediately, we can see that the reconstruction is not flawless. There is an obvious spread about the line of perfect reconstruction, biased towards slower speeds.

For comparison with Figure 2b we have provided an analogous image (Figure 2a) prepared using the smooth multiplicative algebraic reconstruction technique (SMART), the de-facto standard algorithm for inverting MOSES observations. This image is a scatterplot constructed from a single SUMER O III 703.87

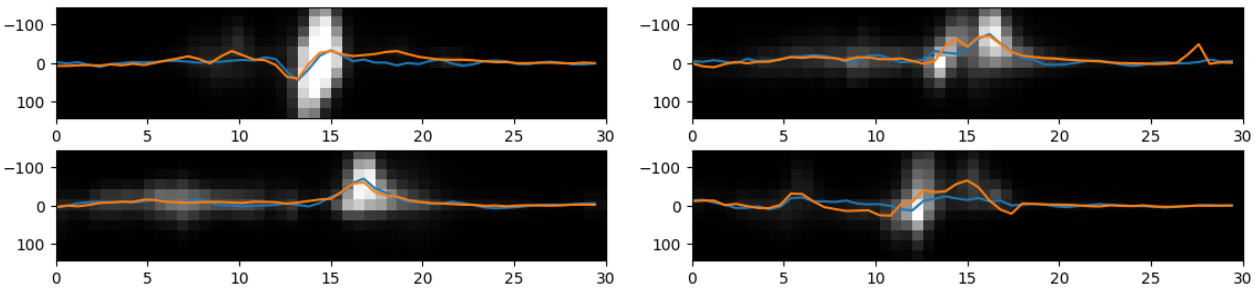


Figure 1: Examples of Doppler inversions. Each image is an IRIS Si IV 1403 Å spectra rebinned into MOSES resolution. The vertical axis is in km/s and the horizontal axis is in arcsec. The true line center is plotted in orange, and the reconstructed line center is plotted in blue.

Å raster. Since Figure 2a is only constructed from a single raster, it contains much less samples than Figure 2b, and therefore the two should not be compared directly. However, SMART's underestimation of velocity is a well-studied phenomenon, so we know that Figure 2a reasonably demonstrates SMART's capabilities.

With the above considerations we can see that according to Figure 2 the DIN is much less likely to underestimate the velocity than this implementation of SMART. However these results are still preliminary and obviously need to be verified by applying SMART to the same IRIS dataset used to validate the DIN.

A quantitative test that we preformed on Figure 2b was the calculation of Pearson's $r$, a test of linearity. The result, enumerated in Table 1 as $r = 0.701$, we interpret as modest performance, likely polluted by spikes in the input dataset.

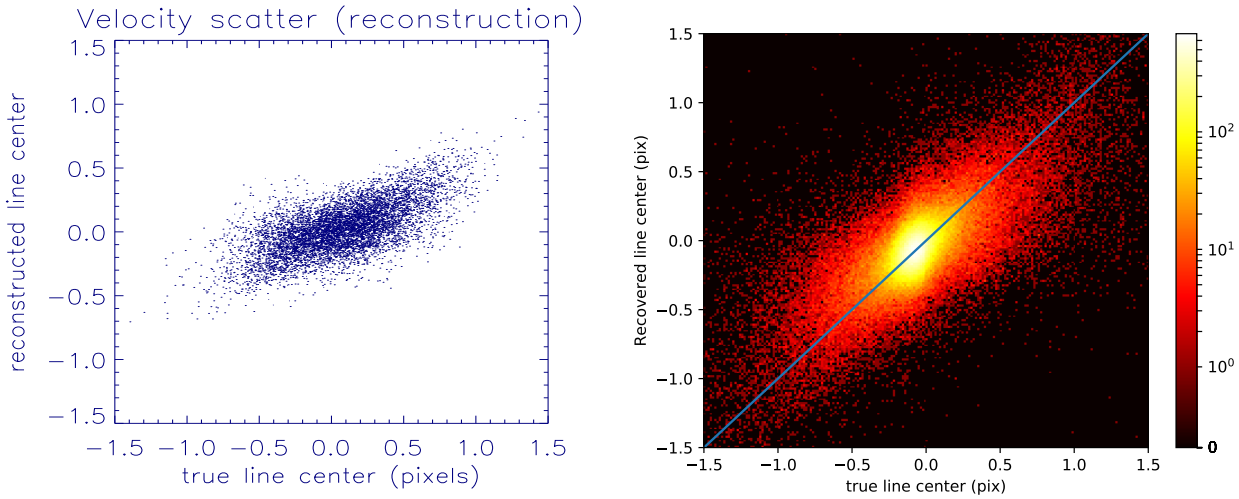


(a) SMART

(b) DIN

Figure 2: Reconstructed vs. true Doppler velocity using both the standard SMART algorithm (applied to SUMER O III 703.87 Å raster; courtesy of Charles Kankelborg), and the CINN algorithm (applied to IRIS Si IV 1403 Å.)

### 2.1.2 Despiking Training Data

Spikes in IRIS observations are a stochastic process, primarily due to ionospheric particles impacting the CCD detectors. Removal of spikes in our training dataset is important since the network will become distracted trying to reconstruct the spikes, a futile undertaking. This was not considered to be a serious problem during the proposal phase, as there have been several despiking routines written for IRIS. However

we failed to appreciate how difficult it would be to apply these routines in an automated fashion to a large section of the IRIS Si IV 1403 Å dataset.

There are a multitude of despiking routines available on the IDL SolarSoft libraries, such as `nospike.pro`, `array_despike.pro`, `despike.pro`. Unfortunately they all identify spikes using the same method: convolution of some kernel with an image to estimate a local mean and standard deviation, and a hard threshold to exclude pixels some number of standard deviations above the mean. This method is often too aggressive in areas of high signal intensity and not aggressive enough in areas of low signal intensity. To use these procedures, we found that we would have to manually tune them for each observation, which would become prohibitive for a large training dataset.

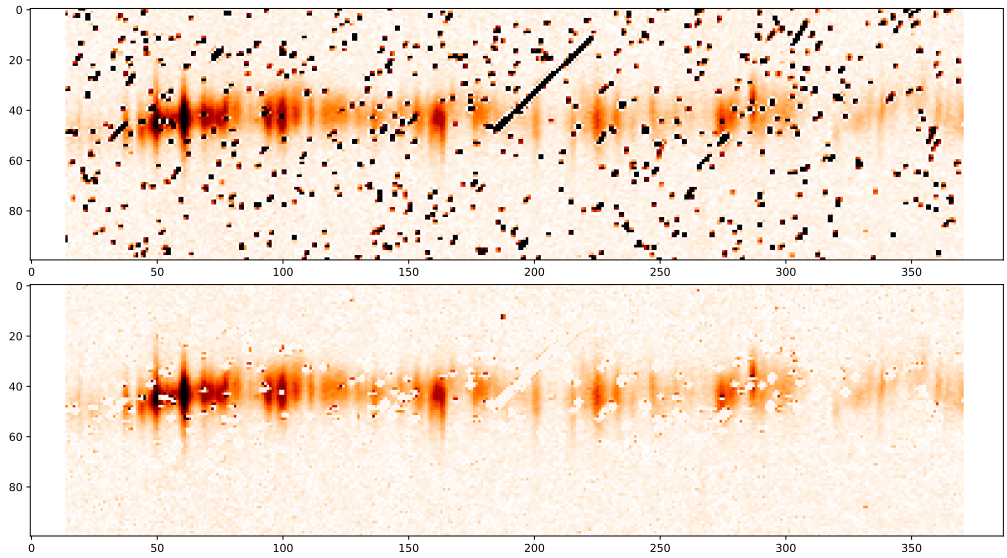

Figure 3: An example of our despiking algorithm applied to an IRIS Si IV 1403 Å spectra, the 47th frame of the observation gathered at 07:24:26 on 06-16-2015. The top image is the original data, and the bottom image is the original data with the identified spikes set to zero. This frame

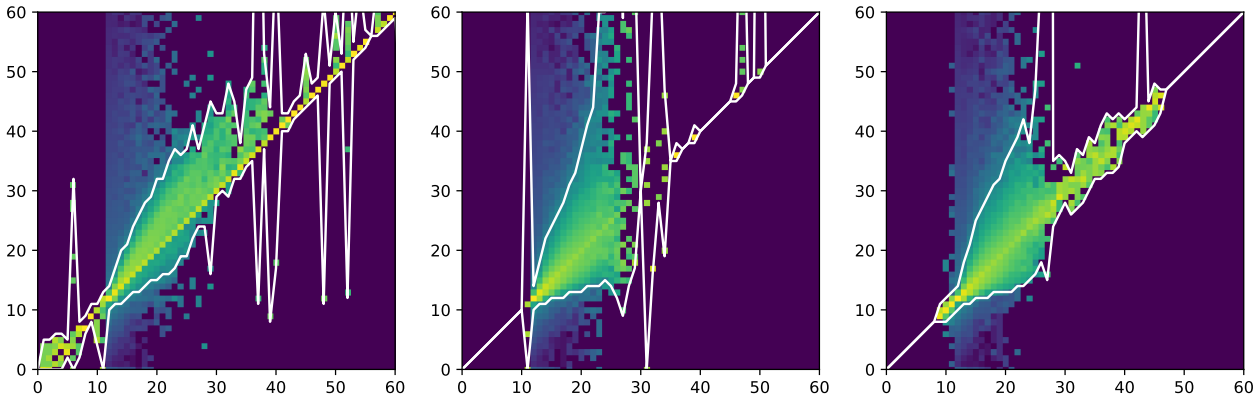

Figure 4

### 2.2 MOSES/ESIS Preparation

### 2.3 FURST Design

## 3 Proposal for Renewal

### 3.1 Further CINN Development

#### 3.1.1 Training Data Pipeline

#### 3.1.2 Quantile Inversion Network

### 3.2 Generative-Adversarial Networks

### 3.3 Explosive Event Classification

### 3.4 MOSES/ESIS Launch

### 3.5 Publications

## 4 Conclusion